This is the manuscript version of „Voňavková T., Horný L. (2019) Effect of axial prestretch and adipose tissue on the inflation-extension behavior of the human abdominal aorta. Computer Methods in Biomechanics and Biomedical Engineering, in press. Publishers version is available via https://dx.doi.org/10.1080/10255842.2019.1699544

Effect of axial prestretch and adipose tissue on the inflation-extension behavior of the human abdominal aorta

Tereza Voňavková[1], Lukáš Horný[*1]

[1]Czech Technical University in Prague, Faculty of Mechanical Engineering, Technická 4, 160 00, Prague, Czech Republic
*Corresponding author: Lukáš Horný, Lukas.horny@fs.cvut.cz

Abstract

Our study aims to show that perivascular adipose tissue may significantly change the mechanical state of the abdominal aorta. To this end, uniaxial tensile tests with perivascular fat tissue were carried out. In the subsequent regression analysis, stress-strain data were fitted by the polynomial strain energy density. A constitutive model of adipose tissue was used in the analytical simulation of the inflation-extension behavior of the human abdominal aorta. The computational model was based on the theory of the bi-layered thick-walled tube. In addition to the effect of perivascular tissue, the effect of axial prestretch was also studied. It was found that the presence of perivascular tissue reduces the distensibility of the aorta. Axial prestretch applied to the aorta embedded in adipose tissue had an effect opposite to that of adipose tissue. Axially prestrained aorta exhibited higher distensiblity than non-prestrained aorta. It was also shown that the perivascular envelope bears some portion of the pressure loading and thus reduces the mechanical stresses inside the wall of aorta. A similar effect was found for axial prestretch.

Keywords: Adipose tissue, aorta, axial prestretch, constitutive model, hyperelasticity, thick-walled tube.

1. Introduction

Despite significant progress that has been achieved in arterial biomechanics in the last few decades, there are still topics that seem to have been overlooked for a long time. In the authors' opinion, one of these is the role of perivascular adipose tissue (PVAT). It may have been a widely accepted idea that perivascular tissue provides mechanical support to an artery, but it has led to a clear oversimplification in which one imagines the role of perivascular adipose tissue in the way that it merely fills the space between the external surface of the artery and neighboring organs. The current anatomical view of the role of PVAT is, however, quite different. Similar to the endothelium, PVAT can modulate vascular tone by releasing vasoactive molecules (Zaborska et al., 2017) which has a direct impact on the mechanical state of the artery. In contrast to the endothelium, PVAT consists of multiple cell types. Besides adipocytes, macrophages, fibroblasts, lymphocytes, and adipocyte progenitor cells are also present in PVAT. The presence of these types of cells suggests the complex endocrine function of PVAT and its contribution to inflammatory processes occurring in the arterial wall (Zaborska et al., 2017; Brown et al., 2014). Considering this, one sees that PVAT is not merely a mechanical support, nor a simple energy-storing tissue, but it is an element with its own complex mechanobiological role.

Nevertheless, it is not only the biological function of PVAT that seems to be underrated in the scientific literature. Computational simulations describing arterial biomechanics considering the effect of perivascular tissue are also rare. If the effect of perivascular tissue is considered, it is most frequently reduced to a form of the boundary condition imposed at the external surface of the artery. This approach has been adopted by Moireau et al. (2012) who investigated the effect of the surrounding tissue on hemodynamics in the aorta, and by Hodis and Zamir (2011) who investigated the effect of external tethering of the arterial wall on the dynamics of pressure pulse transmission.

Liu et al. (2007) obtained pressure-radius experimental data from swine carotid and femoral arteries in the tethered state and after PVAT excision. They showed that arteries with surrounding tissue sustain lower strains and stresses during inflation than their untethered counterparts. Masson et al. (2011) considered perivascular support in their computational model when estimating the constitutive parameters of human carotid arteries from in vivo data. They used the model of the thick-walled tube for the artery; however, the perivascular tissue was again reduced only to its mechanical interaction with the wall by a nonzero external pressure acting on the artery by means of the mathematical expression for perivascular pressure proposed by Humphrey and Na (2002).

One obvious barrier to considering PVAT in computational simulations as a 3D object is the fact that such an object has to be characterized with a constitutive model. However, current scientific literature describing the elastic properties of PVAT at finite strains is very poor. Most of the available experiments have been conducted with subcutaneous adipose tissue, usually from the abdominal region or from the breast, because their primary goal was to provide data suitable for computational simulations focused on plastic and reconstructive surgery (Sommer et al., 2013; Omidi et al., 2014). Moreover, most of these

studies adopted the linear model and describe the elasticity of adipose tissue by means of the Young modulus (Geerligs et al., 2008; Comley and Fleck, 2010). The framework of nonlinear elasticity was adopted by Sommer et al. (2013), Omidi et al. (2014), and Calvo-Galleo et al. (2018), but they did not focus on perivascular tissue.

The goal of the present study is to extend our knowledge of the mechanical behavior of perivascular adipose tissue and its role in the biomechanics of the human abdominal aorta. To this end, uniaxial tensile tests with retropenitonal adipose tissue were carried out. Subsequently, the bi-layer, thick-walled tube analytical model was employed to simulate the effect of the thickness of PVAT and axial prestretch on the mechanical response of the aorta.

2. Materials and Methods

2.1 Tensile testing of adipose tissue

Samples. Specimens were obtained from cadavers autopsied in the Department of Forensic Medicine of Královské Vinohrady University Hospital in Prague. The post-mortem usage of human tissue was approved by the Ethics Committee of the Third Faculty of Medicine of Charles University in Prague. Figure 1 shows the aorta surrounded by adipose tissue. Approximately rectangular strips with typical dimensions of 10 mm x 10 mm x 50 mm were prepared using a scalpel. The reference dimensions of the samples were determined by an image analysis of digital photographs (NIS-Elements, Nikon Instruments). Due to high compliance and the slipperiness of the tissue, it was not possible to perfectly align the strips in either circumferential or longitudinal directions.

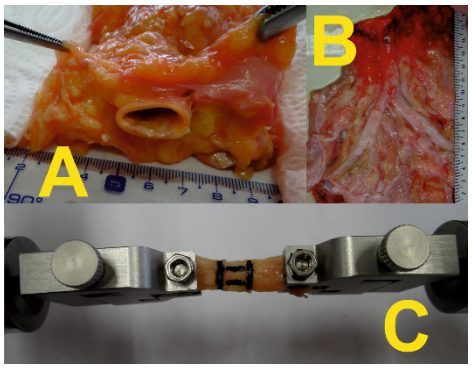

Figure 1. Perivascular tissue surrounds infrarenal aorta – transversal plane (panel A), frontal plane (panel B). A sample of PVAT in uniaxial tension (panel C).

Testing procedure. A multipurpose tensile testing machine (Zwick/Roell, Germany) was used. The testing machine used electromechanical actuators with a displacement resolution of ± 1 μm and U9B force transducers (HBM, Germany, ± 25 N). During the test, the deformation of samples was determined with a built-in videoextensometer by means of contrasting marks created on a sample with liquid eyeliner. The experimental protocol consisted of four cycles as a preconditioning of tissue behavior, and

the fifth cycle was used in the subsequent determination of the material parameters. The loading part of the force–elongation response was used for this purpose. All tests were conducted at room temperature with the velocity of clamps set to 0.2 mms^{-1}.

2.2 PVAT constitutive model and its parameters

Kinematics. It was assumed that during the uniaxial tensile test, the portion of the sample restricted by marks undergoes homogenous dilatation expressed in Cartesian coordinates as $x_i = \lambda_{iK} X_K$ for i, $K = 1, 2,$ and 3 where $\lambda_{iK} = 0$ for $i \neq K$. Here $\boldsymbol{X} = (X_1, X_2, X_3)^T$ and $\boldsymbol{x} = (x_1, x_2, x_3)^T$ respectively denote the position vector in the reference and in the deformed configuration. Deformation gradient $\mathbf{F}$ is defined in (1), and the right Cauchy-Green strain tensor $\mathbf{C}$ is given by $\mathbf{C} = \mathbf{F}^T\mathbf{F}$.

$$\mathbf{F} = \frac{\partial \boldsymbol{x}}{\partial \boldsymbol{X}} \tag{1}$$

Due to high lipid content in the adipose tissue, it is assumed that PVAT is incompressible (Comley and Fleck, 2010; Sommer et al., 2013), thus $det(\mathbf{F}) = 1$ holds during the deformation.

Constitutive model. Since our aim was to use data characterizing PVAT in time-independent (quasi-static) simulations of the inflation-extension behavior of the abdominal aorta, we restricted our attention to the elastic response of PVAT. This means that viscoelastic effects like stress relaxation and creep, which may accompany in vivo pressure wave propagation, are neglected here. Thus perivascular adipose tissue was considered to be hyperelastic (Sommer et al., 2013; Omidi et al., 2014). It was characterized with the strain energy density function expressed in (2). Here c_1, and c_2 denote stress-like material parameters, and I_1 is the first invariant of the right Cauchy-Green deformation tensor $\mathbf{C}$. The isotropic elastic potential (2) was chosen in accordance with Omidi et al. (2014). An assumption of isotropy was adopted, because we were not able to perfectly align samples with their anatomical directions.

$$W_{PT} = c_1\left(I_1 - 3\right) + c_2\left(I_1 - 3\right)^2 \tag{2}$$

The hyperelastic constitutive equation for incompressible material is given by (3). Here $\boldsymbol{\sigma}$ denotes the Cauchy stress tensor, and $\mathbf{I}$ is the second order unit tensor. The symbol p denotes the indeterminate multiplier related to the hydrostatic part of the stress tensor.

$$\boldsymbol{\sigma} = \frac{\partial W}{\partial \mathbf{F}}\mathbf{F}^T - p\mathbf{I} \tag{3}$$

Regression analysis. Experimental stress was obtained as $\sigma_{11}^{EXP} = F\lambda_{11}/S$, where S denotes the reference cross-section area and F is the force elongating the sample from reference length L to deformed length l; $\lambda_{11} = l/L$. The stress predicted by the model, σ_{11}^{MOD}, is obtained from (3), and its final expression is given in (4).

$$\sigma_{11}^{MOD} = 2\left(c_1 + 2c_2\left(\lambda_{11}^2 + \frac{2}{\lambda_{11}} - 3 \right)\right)\left(\lambda_{11}^2 - \frac{1}{\lambda_{11}} \right) \tag{4}$$

2.3 Constitutive model for abdominal aorta

The abdominal aorta wall was modeled as a homogenous, anisotropic, incompressible and hyperelastic continuum characterized by the strain energy density function W_A proposed by Gasser et al. (2006). It is expressed in (5).

$$W_A = \frac{\mu}{2}(I_1 - 3) + \sum_{i=4,6} \frac{k_1}{2k_2}\left(e^{k_2(K_i-1)^2} - 1 \right) \tag{5}$$

$$K_i = \kappa I_1 + (1 - 3\kappa) I_i \qquad i = 4,6 \tag{6}$$

The elastic potential (5) consists of an isotropic part, it is a neo-Hookean term depending on the first invariant of **C**, and an anisotropic exponential part that depends on generalized structural deformation invariants denoted K_4 and K_6. The isotropic part is related to the elastic energy stored in the non-collagenous part of the arterial wall, whereas the anisotropic part is linked to the energy stored in bundles of collagen fibers. Since these fibers have a stochastic wavy pattern, their recruitment into the load-bearing process results in the strain-stiffening response, which is well described by an exponential function (Holzapfel et al., 2000). The model is based on the assumption that bundles of collagen fibers are arranged in the arterial wall with two dominant helices wound around the longitudinal axis at angles of $\pm(90° - \beta)$. These helices can be in cylindrical coordinates (R, Θ, Z) characterized with unit vectors $\boldsymbol{M}_1 = (0, cos(\beta), sin(\beta))^T$, $\boldsymbol{M}_2 = (0, cos(-\beta), sin(-\beta))^T$. These preferred directions give rise to deformation invariants I_4 and I_6 according to (7).

$$I_4 = \boldsymbol{M}_1 \cdot (\mathbf{C}\boldsymbol{M}_1) = \boldsymbol{M}_2 \cdot (\mathbf{C}\boldsymbol{M}_2) = I_6 \tag{7}$$

In fact, however, the collagen fibers are not perfectly aligned with the directions $\boldsymbol{M}_1$ and $\boldsymbol{M}_2$. Rather, they exhibit some dispersion around the predominant directions. The used strain energy function takes this into account by using generalized structural invariants K_4 and K_6 that also include a contribution from invariant I_1. Nevertheless, it is worth noting that, although the model (5) enables structural interpretation, in fact it is a phenomenological model, and its parameters should not be confused with the exact internal architecture of the arterial wall.

2.4 Simulation of the inflation-extension behavior of the abdominal aorta with PVAT

Geometry and kinematics. The abdominal aorta was modeled as a homogenous thick-walled tube with the reference geometry corresponding to an open cylinder to take into account circumferential residual

strains (Horný et al., 2014 a, b). Hence in the first step, the reference stress-free opened cylinder is closed to form a hollow cylinder. The kinematics in polar cylindrical coordinates is expressed in equations (8). (ρ, ϑ, ζ) are coordinates defined in the stress-free configuration, whereas (R, Θ, Z) are defined in the residually stressed but unpressurized state. In equations (8b) and (8c), α is the opening angle, and δ is the axial stretch accompanying closing into a cylindrical geometry.

$$R = R(\rho) \qquad \Theta = 2\pi/(2\pi - 2\alpha)\vartheta \qquad Z = \delta\zeta \tag{8}$$

Subsequently, the aorta is elongated by axial force F_{red} to reach its in situ length, and inflation by internal pressure P follows. During pressurization, the aorta can further elongate or shorten, and that is governed by equilibrium equations. In (9), the deformed configuration is expressed in the polar cylindrical coordinates (r, θ, z).

$$r = r(R) \qquad \theta = \Theta \qquad z = \lambda Z \tag{9}$$

The total deformation gradient of the aorta $\mathbf{F}_A$ is then given as $\mathbf{F}_A = \mathbf{F}_{A2}\mathbf{F}_{A1}$, where $\mathbf{F}_{A1}$ is linked to the residual deformation and $\mathbf{F}_{A2}$ expresses subsequent inflation and extension. The matrices of the gradients are given in (10) and (11).

$$\mathbf{F}_A = \mathbf{F}_2\mathbf{F}_1 = \begin{pmatrix} \lambda_{r\rho} & 0 & 0 \\ 0 & \lambda_{\theta\vartheta} & 0 \\ 0 & 0 & \lambda_{z\zeta} \end{pmatrix} = \begin{pmatrix} \partial r/\partial\rho & 0 & 0 \\ 0 & \pi r/[\rho(\pi-\alpha)] & 0 \\ 0 & 0 & \lambda\delta \end{pmatrix} \tag{10}$$

$$\mathbf{F}_{A1} = \begin{pmatrix} \lambda_{R\rho} & 0 & 0 \\ 0 & \lambda_{\Theta\vartheta} & 0 \\ 0 & 0 & \lambda_{Z\zeta} \end{pmatrix} = \begin{pmatrix} \partial R/\partial\rho & 0 & 0 \\ 0 & \pi R/[\rho(\pi-\alpha)] & 0 \\ 0 & 0 & \delta \end{pmatrix} \tag{11}$$

$$\mathbf{F}_{A2} = \begin{pmatrix} \lambda_{rR} & 0 & 0 \\ 0 & \lambda_{\theta\Theta} & 0 \\ 0 & 0 & \lambda_{zZ} \end{pmatrix} = \begin{pmatrix} \partial r/\partial R & 0 & 0 \\ 0 & r/R & 0 \\ 0 & 0 & \lambda \end{pmatrix} \tag{12}$$

To account for the effect of perivascular tissue on the mechanics of the aorta, it is assumed that during its inflation and extension the aorta is surrounded by an external cylindrical layer composed of PVAT. $R_{oA} = R_{iPT}$ and $r_{oA} = r_{iPT}$ hold during the deformation. Here R_{iPT} and r_{iPT} denote the reference and deformed inner radius of the PVAT cylinder, Figure 2. It is assumed that the PVAT cylinder retains its cylindrical shape in the deformation, thus its deformation gradient has a form similar to $\mathbf{F}_{A2}$.

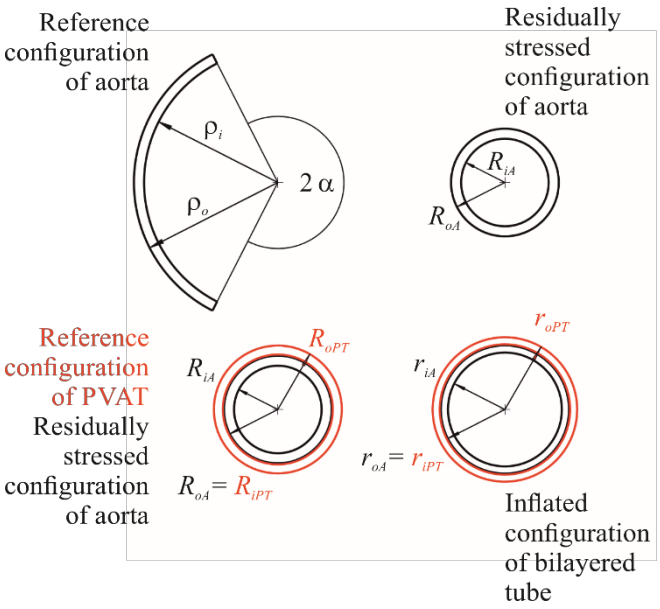

Figure 2. Reference and deformed configurations.

Equilibrium equations. Equilibrium equations for the bi-layered tube can be written in the forms (13-14). Here $\hat{W}$ denotes W with radial stretch being substituted from the incompressibility condition. W_A represents the strain energy stored in the aorta (5), and W_{PT} denotes the energy stored in PVAT (2).

$$P = \int_{r_{iA}}^{r_{oA}} \lambda_{\theta\vartheta} \frac{\partial \hat{W}_A}{\partial \lambda_{\theta\vartheta}} \frac{dr}{r} + \int_{r_{iPT}}^{r_{oPT}} \lambda_{\theta\Theta} \frac{\partial \hat{W}_{PT}}{\partial \lambda_{\theta\Theta}} \frac{dr}{r} \tag{13}$$

$$F_{red} = \pi \int_{r_{iA}}^{r_{oA}} \left(2\lambda_{z\zeta} \frac{\partial \hat{W}_A}{\partial \lambda_{z\zeta}} - \lambda_{\theta\vartheta} \frac{\partial \hat{W}_A}{\partial \lambda_{\theta\vartheta}} \right) r dr + \pi \int_{r_{iPT}}^{r_{oPT}} \left(2\lambda_{zZ} \frac{\partial \hat{W}_{PT}}{\partial \lambda_{zZ}} - \lambda_{\theta\Theta} \frac{\partial \hat{W}_{PT}}{\partial \lambda_{\theta\Theta}} \right) r dr \tag{14}$$

Equations (13) and (14) assume that the boundary conditions $\sigma_{rr}(r_{iA}) = -P \wedge \sigma_{rr}(r_{oPT}) = 0$ hold. The tube is considered to be closed, and F_{red} is an additional axial force which ensures the initial axial stretch ($\lambda_{z\zeta}^{ini}$) and which the aorta sustains independently of internal pressure P (Horný et al., 2013, 2014b, 2017).

2.5 Stress distribution through the wall

To evaluate stress distribution through the wall, equations (15a), (15b), and (15c) have been adopted. Stresses acting in PVAT are obtained when substitution from (2) is performed, and $\lambda_{\theta\Theta}$, λ_{zZ}, and integration to r_{oPT} is considered.

$$\sigma_{rr}(r) = -\int_{r}^{r_{oA}} \lambda_{\theta\vartheta} \frac{\partial \hat{W}_A}{\partial \lambda_{\theta\vartheta}} \frac{dx}{x} - \int_{r_{iPT}}^{r_{oPT}} \lambda_{\theta\Theta} \frac{\partial \hat{W}_{PT}}{\partial \lambda_{\theta\Theta}} \frac{dr}{r} \qquad \sigma_{\theta\theta}(r) = \lambda_{\theta\vartheta} \frac{\partial \hat{W}_A}{\partial \lambda_{\theta\vartheta}} + \sigma_{rr} \qquad \sigma_{zz}(r) = \lambda_{z\zeta} \frac{\partial \hat{W}_A}{\partial \lambda_{z\zeta}} + \sigma_{rr} \tag{15}$$

2.6 Thickness of PVAT, loading conditions and material parameters

PVAT thickness. With regard to the amount of fat tissue, anatomical variations in the human population are rather large. To take this fact into account, three representative thicknesses of the PVAT layer were considered in our simulations. These cases were chosen with reference to the thickness of the aorta such that: (I) represents a very thin fat layer with 0.2 mm = $H_{PT} \ll R_{oA} - R_{iA}$, (II) $H_{PT} = R_{oA} - R_{iA}$ is the middle case, and (III) $R_{oA} - R_{iA} \ll H_{PT}$ = 40 mm represents a situation in which the movement of aorta is significantly restricted by surrounding tissue.

Loading. External loading during the inflation-extension response of the aorta is represented by internal pressure P and the initial axial stretch $\lambda_{z\zeta}^{ini}$ that the aorta sustains independently of pressure. To account for prestretch, F_{red} necessary to elongate the aorta to $\lambda_{z\zeta}^{ini}$ was computed at P = 0. In the subsequent pressurization from 0 up to 16 kPa, F_{red} was held constant, which ensured that $\lambda_{z\zeta}$ would vary during inflation. Values where $\lambda_{z\zeta}^{ini}$ = 1, 1.1, and 1.2 were considered in our study.

Material parameters for the aorta and PVAT. The material parameters for the abdominal aorta were adopted from Horný et al. (2014a). One representative sample of a 38-year-old male donor was considered (denoted M38). The specific values of the material parameters are provided in Table 1. In contrast to aortic tissue, the PVAT parameters are based on our experiments. In the inflation-extension simulation, average perivascular tissue behavior was considered. Since the constitutive equation for PVAT is nonlinear, the material parameters used in the study were fitted to all the data to obtain a mean model. Such an approach takes into account the effects of all observed responses and naturally produces a model which can be considered an average model.

Table 1 Constitutive parameters and geometry of the human abdominal aorta. Adopted form Horný et al. (2014a).

	Sex	Age [years]	μ [kPa]	k_1 [kPa]	k_2 [–]	κ [–]	β [°]	ρ_i [mm]	ρ_o [mm]	α [°]	R_{iA} [mm]	R_{oA} [mm]
M38	Male	38	15.9	78.49	4.99	0.19	41.41	16.2	17.24	117	5.3	6.52

3. Results and Discussion

3.1 Constitutive behavior of adipose tissue

Fifteen successful uniaxial tensile tests were conducted with samples of PVAT obtained from seven donors. Table 2 summarizes the age, sex, and number of samples obtained from each donor. The samples exhibited a nonlinear response at large strains, Figure 3. The model curves were computed by means of least square optimization for: (a) the most compliant case, (b) with all measured data pooled together

which resulted in the set of material parameters that represents the average mechanical behavior, and finally (c) the stiffest case. The estimated material parameters appear in Table 2.

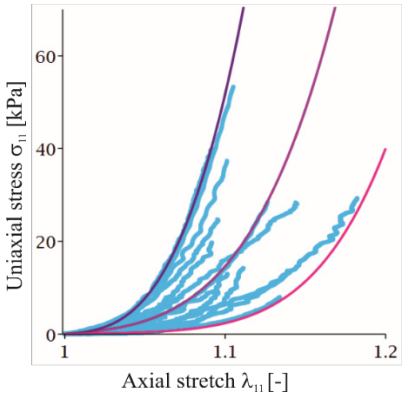

Figure 3. Uniaxial tensile tests of PVAT and model curves.

The uniaxial tensile tests confirmed that the elastic response of PVAT, similar to subcutaneous fatty tissue, is highly nonlinear (Sommer et al., 2013; Calvo-Gallego et al., 2018). Unfortunately, in contrast to Sommer et al. (2013), we cannot conclude that the observed behavior suggests anisotropic material properties, because we were not able to ensure the constant orientation of the samples during their separation. The highly compliant response of the tissue complicated manual preparation.

Omidi et al. (2014) studied the mechanical behavior of adipose tissue in the subcutaneous abdominal region by means of an indentation test. They employed the Yeoh hyperelastic model (third order polynomial in I_1) to express the constitutive properties of the tissue. They arrived at values of the material parameters that seem to be somewhat lower than those found in our study. $c_1 = 0.16$ kPa, $c_2 = 0.018$ kPa, and $c_3 = 1.1 \cdot 10^{-7}$ kPa are typical values estimated by Omidi et al. (2014). This discrepancy may be partially attributed to a different experimental technique used in Omidi et al. (2014), but the most important difference seems to be the fact that Omidi et al. (2014) decellularized the tissue before testing, which can significantly change the mechanical properties of tissues (Bielli et al., 2018; Liao et al., 2008).

Although adipose tissue is very compliant and small values of an acting force can deform such an object to a state which requires employing the finite strain theory, small strain approximations are sometimes used in the literature. In this approach, the framework of linear elasticity is appropriate, and one can find studies reporting values for the Young elastic modulus for adipose tissue. Restricting our attention to the small strain theory, we can substitute the nonlinear model (2) with the slope of the tangent computed to a stress–strain curve at the beginning of the deformation. This slope is referred to as the initial elastic modulus. A consideration of the material parameters presented in Table 2 leads to 0.6 kPa, for the most compliant material response, to 4.3 kPa for an average response, and to 32.7 kPa for the stiffest case. Omidi et al. (2014) reported 3.4 kPa for the Young modulus obtained for abdominal subcutaneous tissue.

Comley and Fleck (2010, 2012), Nightingale et al. (2003), and Miller-Young et al. (2002) reported a Young modulus in the range of 1 – 14 kPa depending on the source of the tissue and the applied strain rate. Geerligs et al. (2008) reported the shear elastic modulus of subcutaneous tissue to be 7.5 kPa, which implies an elastic modulus of about 22 kPa. Thus, we conclude that our data suggest somewhat stiffer behavior for perivascular adipose tissue than is known for subcutaneous tissue; however, under small strains they do not differ significantly.

3.2 Inflation-extension response of abdominal aorta surrounded with adipose tissue

The effect of perivascular adipose tissue on the mechanics of the abdominal aorta was simulated by means of an analytical model based on the bi-layered thick-walled tube problem formulated within a framework of nonlinear elasticity and numerically solved in Maple. Figures 4 and 5 show the resulting inflation and extension behavior in terms of deformed radius and axial stretch obtained for the 38-year-old male individual (M38). To highlight the effect of PVAT and axial prestretch on the circumferential response of the aorta, Figure 6 depicts the dependence between circumferential stretch (computed at r_{iA}) and the inflating pressure. Figures 7 (aorta) and 8 (PVAT) show the stress distribution through the thickness of the wall computed at loading pressure P = 16 kPa for tubes with different H_{PT} and $\lambda_z\zeta^{ini}$.

Table 2. PVAT samples summary and material parameters (a – the most compliant case, b – average model, c – the stiffest case).

Donor	Sex {M,}	Age [years]	n [–]
1	M	71	3
2	M	41	3
3	M	67	2
4	M	71	1
5	F	53	1
6	M	29	3
7	M	69	2

	c_1 [kPa]	c_2 [kPa]
(a)	0.1	89.7
(b)	0.723	418
(c)	5.46	1439

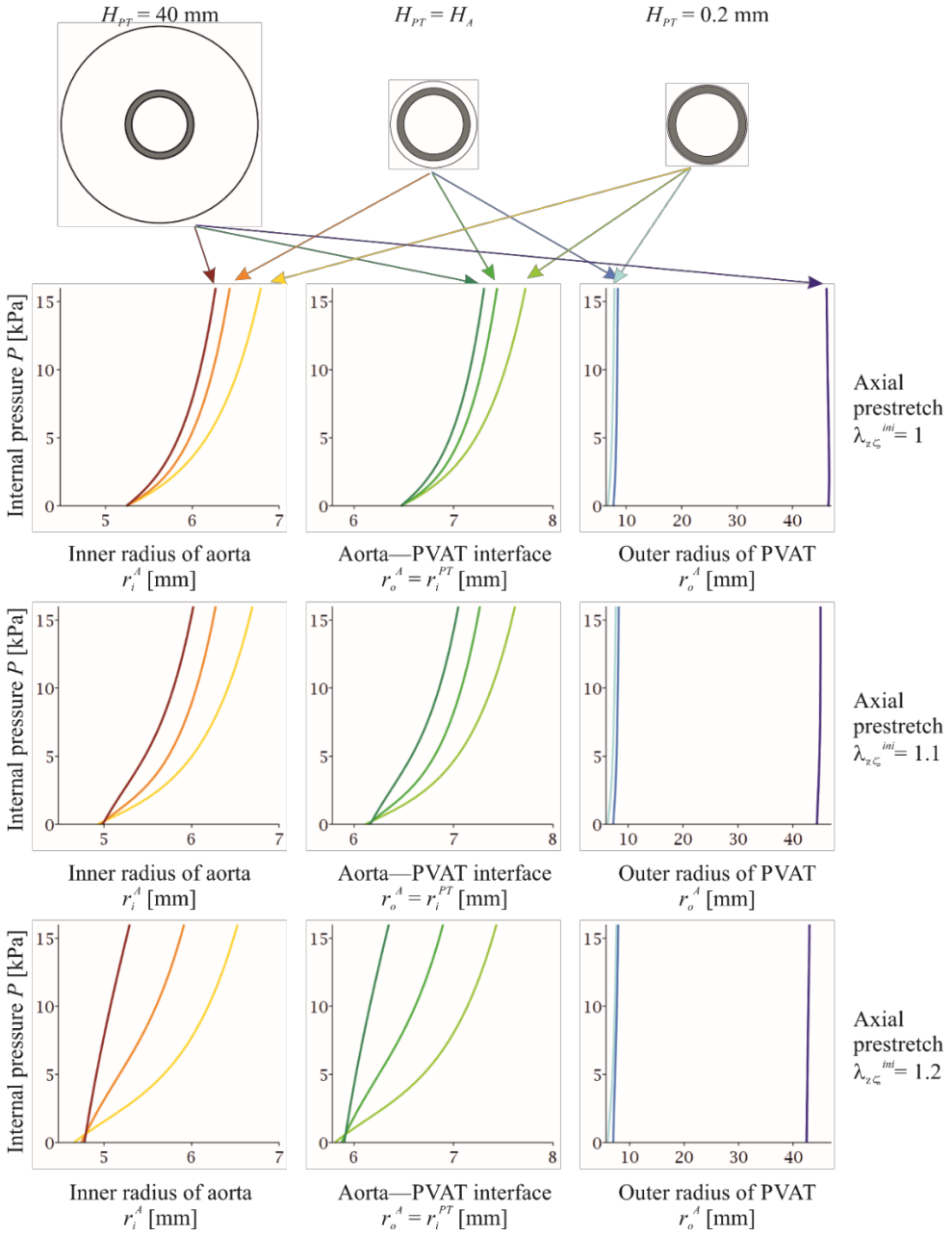

Figure 4. Inflation response of abdominal aorta M38 surrounded by PVAT with H_{PT} = 0.2, 1.22, and 40 mm.

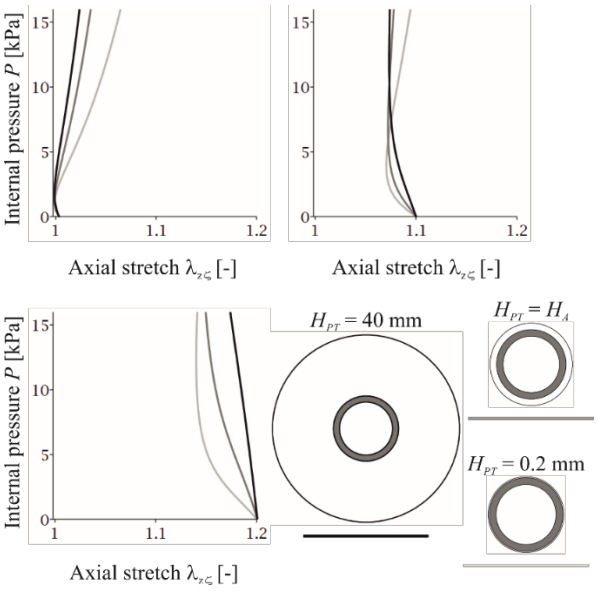

Figure 5. Extension response of abdominal aorta M38 surrounded by PVAT with H_{PT} = 0.2, 1.22, and 40 mm.

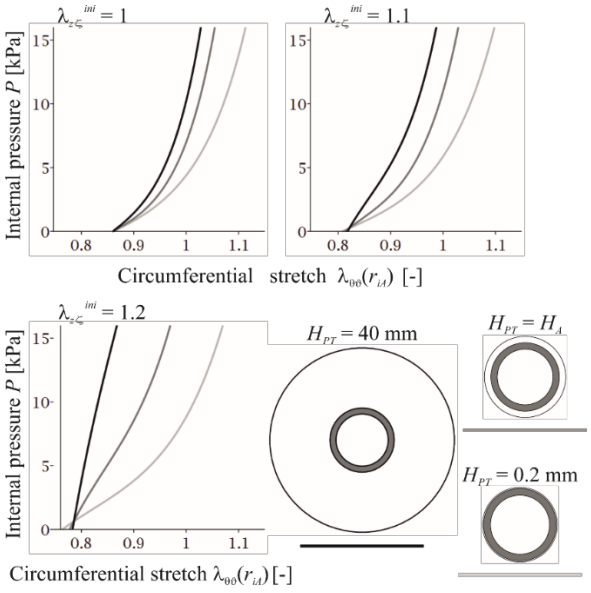

Figure 6. Dependence of circumferential stretch at the inner radius of the aorta during inflation of M38 on axial prestretch.

With regard to inflation behavior, the figures document that PVAT restricts the radial motion of an artery. It is exhibited in each studied position (r_{iA}, $r_{oA} = r_{iPT}$, and r_{oPT}; see Figure 4). Where r_{oPT} for H_{PT} = 40 mm, the movement is almost negligible in comparison with the thickness of the fatty tissue. Thus, one could hypothetically conclude that the presence of the fatty surrounding is mechanically disadvantageous for the human body, because it prevents an artery from functioning as an elastic capacitor in the Windkessel effect. Later, we will see that this is just one side of the coin.

In contrast to PVAT, axial prestretch has, in the range of physiological pressure, the absolutely opposite effect. Figure 4 documents that the $P - r$ responses are more compliant when longitudinal pretension is applied. Perhaps it is most clearly depicted in Figure 6, where circumferential stretch at the inner radius of the aorta is presented. In accordance with our previous study, Horný et al. (2014b), it can be said that the axial prestrain of the tube leads to higher circumferential distensibility in the inflation carried out at physiological pressures. Since the distensibility may not be easily recognized from the figure, Table 3 includes the specific results obtained for H_{PT} and $\lambda_{z\zeta}^{ini}$. The distensibility is quantified as (r_{iA}(16kPa) – r_{iA}(10kPa))/r_{iA}(10kPa). From Table 3, we can conclude that, although increasing H_{PT} leads to decreasing distensibility, axial preloading balances this influence.

Table 3. Specific values of distensibility, (r_{iA}(16kPa) – r_{iA}(10kPa))/r_{iA}(10kPa), obtained from the curves in Figure 6.

	M38	H_{PT} = 0.2 mm	$H_{PT} = H_A$	H_{PT} = 40 mm
$\lambda_{z\zeta}^{ini} = 1$		0.0469	0.0333	0.0279
$\lambda_{z\zeta}^{ini} = 1.1$		0.0521	0.0340	0.0390
$\lambda_{z\zeta}^{ini} = 1.2$		0.0631	0.0612	0.0454

The axial response is depicted in Figure 5. We again observe that including perivascular tissue into the model has, similar to circumferential behavior, an immobilization effect. The dark curves corresponding to H_{PT} = 40 mm exhibit a lower stretch variation, $\lambda_{z\zeta}(P_2) - \lambda_{z\zeta}(P_1)$ for $P_1 < P_2$, than the light curves obtained for the thinner PVAT layers. At typical physiological pressures, P_2 = 16 kPa and P_1 = 10 kPa, it is also visible for $\lambda_{z\zeta}^{ini}$ = 1.1. In this case, the curve corresponding to H_{PT} = 40 mm is almost perpendicular to the horizontal axis of the graph, which suggests that the prestretched tube does not move axially during the pressure pulse. It has been hypothesized in the literature that minimization of the axial movement during the pressure pulse transmission is advantageous for arteries (Schulze-Bauer et al., 2003). Our results show that PVAT contributes to the minimization of axial movement of the aorta.

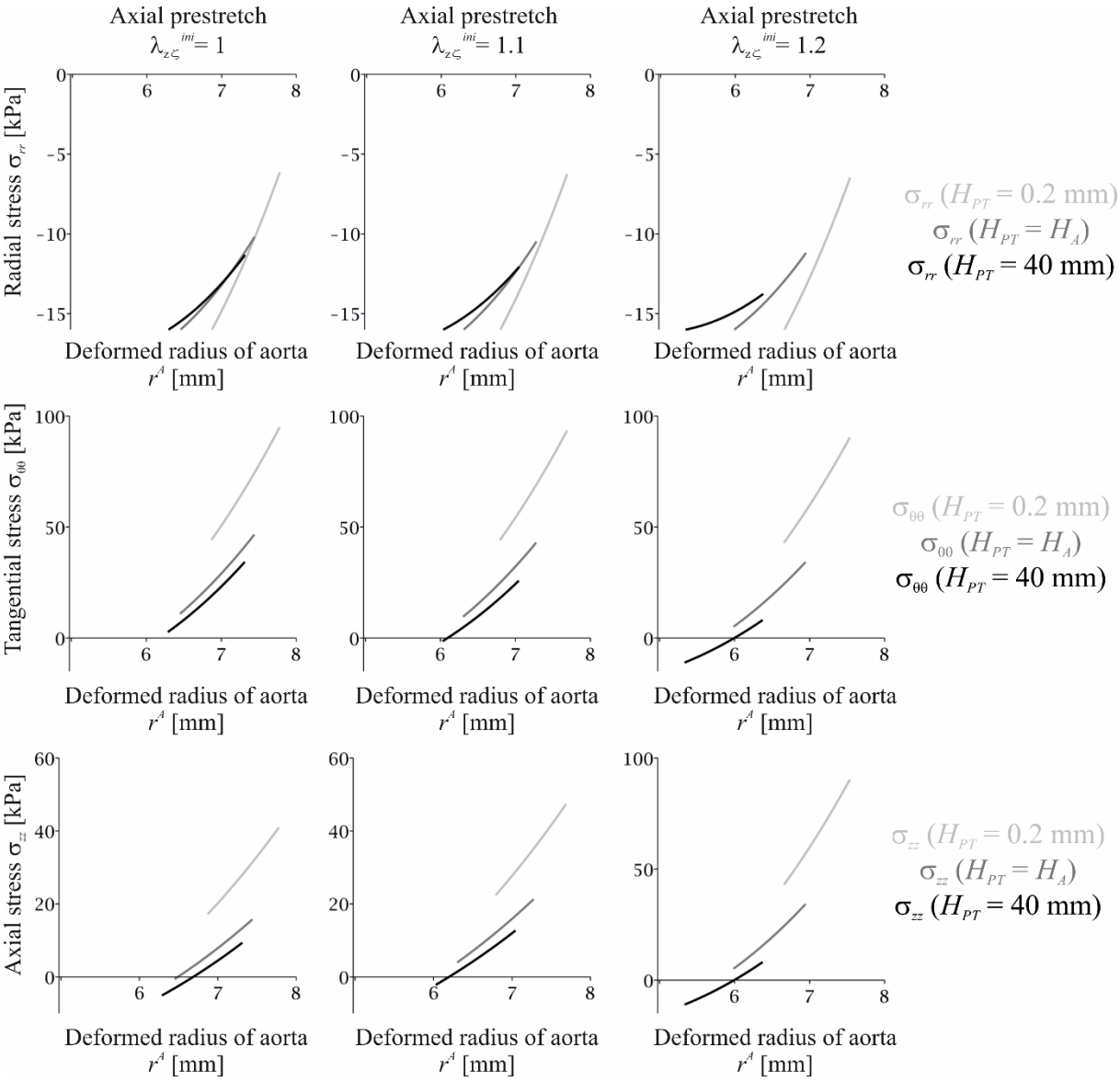

Figure 7. Distribution of in-wall stresses in aorta M38 pressurized to 16 kPa and surrounded by PVAT with H_{PT} = 0.2, 1.22, and 40 mm.

On the other hand, comparing the panels created for $\lambda_{z\zeta}^{ini}$ = 1.2 with panels for $\lambda_{z\zeta}^{ini}$ = 1.1 indicates that this behavior is not monotonic. It does not hold true in the sense that the higher the prestretch the lower the axial movement would generally be. Where $\lambda_{z\zeta}^{ini}$ = 1.2, the lowest variation of axial deformation is obtained for H_{PT} = 0.2 mm. However, human arteries are not prestrained without limits. For the abdominal aorta, typical values can be found in Horný et al. (2014b, 2017). These studies suggest $\lambda_{z\zeta}^{ini}$ = 1.179 for M38 is to be expected. The value comes from the studied interval $\lambda_{z\zeta}^{ini}$ = 1 – 1.2. Computations show that somewhere inside this interval the longitudinal response changes from pressure-induced elongation to pressure-induced shortening. Our results suggest that the expected values of prestretch, presented in Horný et al. (2014b), fall close to a hypothetical optimal point not only in the case of bare aortas but also when the existence of PVAT and its mechanical role are considered.

This is the manuscript version of „Voňavková T., Horný L. (2019) Effect of axial prestretch and adipose tissue on the inflation-extension behavior of the human abdominal aorta. Computer Methods in Biomechanics and Biomedical Engineering, in press. Publishers version is available via https://dx.doi.org/10.1080/10255842.2019.1699544

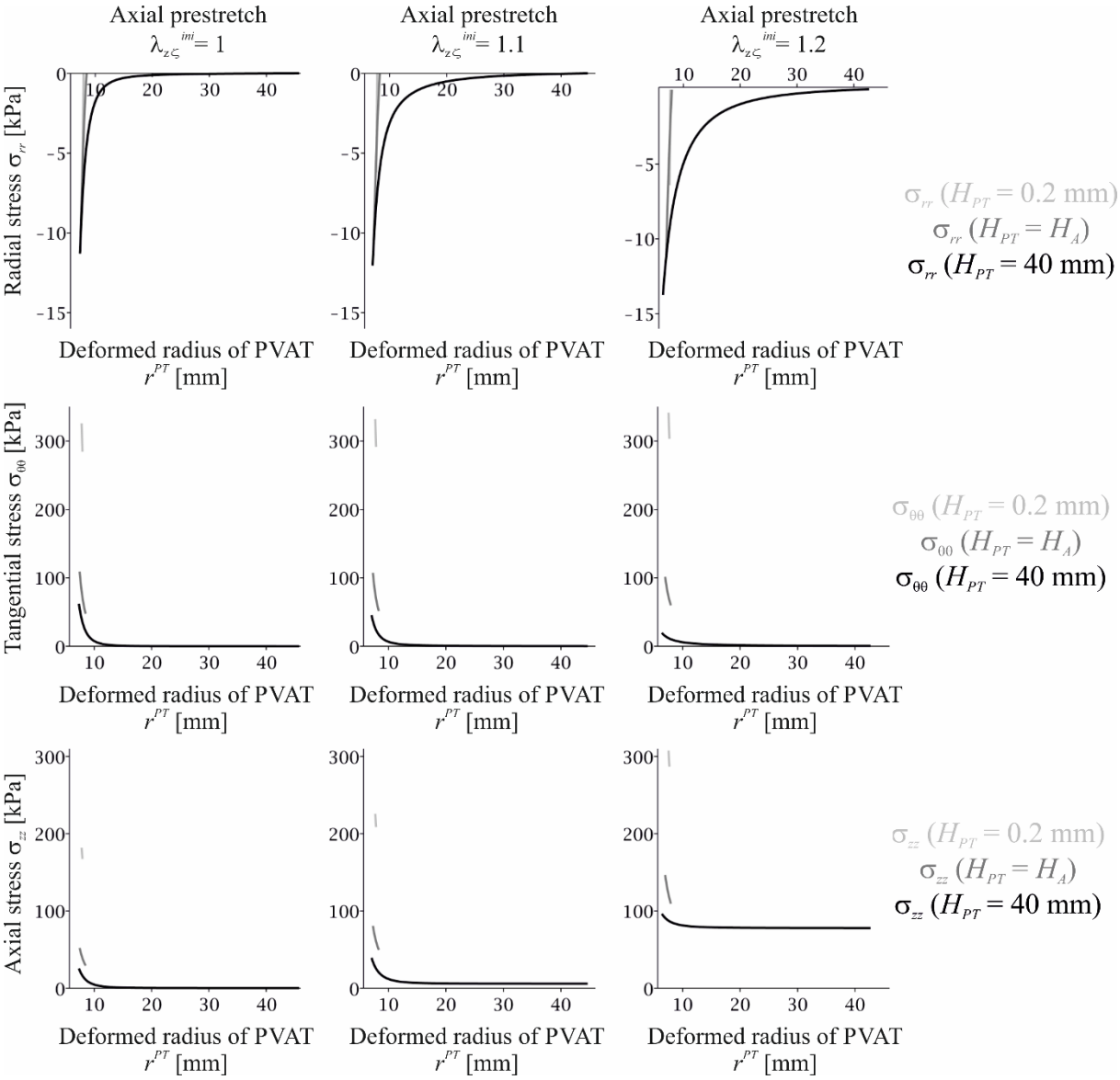

Figure 8. Distribution of in-wall stresses in PVAT at P = 16 kPa. PVAT tube thickness was H_{PT} = 0.2, 1.22, and 40 mm.

In accordance with a solution known from the classical theory of elasticity for the bi-layered thick-walled tube, the computed distribution of radial stress confirms that PVAT bears some portion of the pressure load. Transmural pressure loading PVAT, $-\Delta P_{PT} = \sigma_{rr}(r_{iPT}) - \sigma_{rr}(r_{oPT}) = \sigma_{rr}(r_{iPT})$, increases when the thickness of PVAT increases. Reciprocally, the thicker the PVAT layer is, the lower is the loading of the aorta, $-\Delta P_A = \sigma_{rr}(r_{iA}) - \sigma_{rr}(r_{oA}) = -P + \Delta P_{PT}$. As a consequence of the decreasing loading of the aorta, the increasing thickness of PVAT causes a decrease in circumferential and axial stresses. This is another example showing that the existence of PVAT is advantageous from a mechanical point of view. It bears some portion of the loading and thus decreases the load acting on the aorta itself.

The role of axial prestretch is very interesting. The middle row in Figure 7 shows that increasing axial pretension leads to a decrease in circumferential stress in the aorta. Where $\lambda_{z\zeta}^{ini} = 1.2$ and $H_{PT} = 40$ mm, negative values for $\sigma_{\theta\theta}$ at r_{iA} are even reached. Interestingly, in the PVAT layer, an increase in circumferential stress at r_{iPT} is observed for $H_{PT} = 0.2$ (Figure 8). However, the maximum value of circumferential stress decreases with increasing $\lambda_{z\zeta}^{ini}$ for $H_{PT} = H_A$ and $H_{PT} = 40$ mm. This documents that the effect of axial pretension is not monotonic with respect to the simultaneous effect of the thickness.

4. Conclusion

Constitutive parameters of perivascular adipose tissue were found in our study. A hyperelastic constitutive description was employed in the form of the polynomial strain energy density. The obtained material parameters were subsequently used in the analytical solution of the bi-layer thick-walled tube problem simulating the mechanical effect of PVAT on the abdominal aorta. Simultaneous with examining the effect of PVAT, the effect of axial prestretch was also studied. It was found that the presence of PVAT reduces distensibility. Axial prestretch applied to the aorta embedded in PVAT had an opposite effect. Axially prestrained aortas exhibited higher distensiblity than non-prestrained aortas. It was also shown that the perivascular envelope bears some portion of the pressure loading and thus reduces the mechanical stresses inside the wall of the aorta. A similar effect was found for axial prestretch. The results suggest that perivascular adipose tissue is mechanically advantageous, due to it reducing wall stresses, and that decreased arterial distensibilty is compensated for by axial prestretch in the aorta.

Acknowledgement

This study has been financially supported by the Czech Science Foundation in the grant project no. GA18-26041S “Effect of axial prestretch on mechanical response of nonlinearly elastic and viscoelastic tubes”.

References

Bielli A, Bernardini R, Varvaras D, Rossi P, Di Blasi G, Petrella G, Buonomo OC, Mattei M, Orlandi A. Characterization of a new decellularized bovine pericardial biological mesh: Structural and mechanical properties. J Mechan Behav Biomed Mater 2018;78:420-426.

Brown NK, Zhou Z, Zhang J, Zeng R, Wu J, Eitzman DT, Chen YE, Chang L. Perivascular adipose tissue in vascular function and disease: A review of current research and animal models. Arterioscler Thromb Vasc Biol 2014;34:1621-1630.

Calvo-Gallego JL, Domínguez J, Gómez Cía T, Gómez Ciriza G, Martínez-Reina J. Comparison of different constitutive models to characterize the viscoelastic properties of human abdominal adipose tissue. A pilot study. J Mechan Behav Biomed Mater 2018;80:293-302.

Comley K, Fleck NA. A micromechanical model for the young's modulus of adipose tissue. Int J Solids Struct 2010;47:2982-2990.

Comley K, Fleck N. The compressive response of porcine adipose tissue from low to high strain rate. Int J Impact Eng 2012;46:1-10.

Gasser TC, Ogden RW, Holzapfel, GA. Hyperelastic modelling of arterial layers with distributed collagen fibre orientations. J Royal Soc Interface 2006;3:15-35.

Geerligs M, Peters GWM, Ackermans PAJ, Oomens CWJ, Baaijens FPT. Linear viscoelastic behavior of subcutaneous adipose tissue. Biorheology 2008;45:677-688.

Hodis S, Zamir M. Mechanical events within the arterial wall under the forces of pulsatile flow: A review. J Mechan Behav Biomed Mater 2011;4:1595-1602.

Holzapfel GA, Gasser TC, Ogden RW. A new constitutive framework for arterial wall mechanics and a comparative study of material models. J Elast 2000;61:1-48.

Horny L, Adamek T, Zitny R. Age-related changes in longitudinal prestress in human abdominal aorta. Arch Appl Mech 2013;83:875-888.

Horný L, Netušil M, Daniel M. Limiting extensibility constitutive model with distributed fibre orientations and ageing of abdominal aorta. J Mechan Behav Biomed Mater 2014;38:39-51.

Horný L, Netušil M, Voňavková T. Axial prestretch and circumferential distensibility in biomechanics of abdominal aorta. Biomech Model Mechanobiol 2014;13:783-799.

Horný L, Adámek T, Kulvajtová M. A comparison of age-related changes in axial prestretch in human carotid arteries and in human abdominal aorta. Biomech Model Mechanobiol 2017;16:375-383.

Humphrey JD, Na S. Elastodynamics and arterial wall stress. Ann Biomed Eng 2002;30:509-523.

Liao J, Joyce EM, Sacks MS. Effects of decellularization on the mechanical and structural properties of the porcine aortic valve leaflet. Biomaterials 2008;29:1065-1074. Liu Y, Dang C, Garcia M, Gregersen H, Kassab GS. Surrounding tissues affect the passive mechanics of the vessel wall: Theory and experiment. Am J Physiol - Heart Circ Physiol 2007;293:H3290-H3300.

Masson I, Beaussier H, Boutouyrie P, Laurent S, Humphrey JD, Zidi M. Carotid artery mechanical properties and stresses quantified using in vivo data from normotensive and hypertensive humans. Biomech Model Mechanobiol 2011;10:867-882.

Miller-Young JE, Duncan NA, Baroud G. Material properties of the human calcaneal fat pad in compression: Experiment and theory. J Biomech 2002;35:1523-1531.

Moireau P, Xiao N, Astorino M, Figueroa CA, Chapelle D, Taylor CA, Gerbeau J. External tissue support and fluid-structure simulation in blood flows. Biomech Model Mechanobiol 2012;11:1-18.

Nightingale K, McAleavey S, Trahey G. Shear-wave generation using acoustic radiation force: In vivo and ex vivo results. Ultrasound Med Biol 2003;29:1715-1723.

Omidi E, Fuetterer L, Reza Mousavi S, Armstrong RC, Flynn LE, Samani A. Characterization and assessment of hyperelastic and elastic properties of decellularized human adipose tissues. J Biomech 2014;47:3657-3663.

Schulze-Bauer CAJ, Mörth C, Holzapfel GA. Passive biaxial mechanical response of aged human iliac arteries. J Biomech Eng 2003;125:395-406. https://doi.org/10.1115/1.1574331

Sommer G, Eder M, Kovacs L, Pathak H, Bonitz L, Mueller C, Regitnig P, Holzapfel GA. Multiaxial mechanical properties and constitutive modeling of human adipose tissue: A basis for preoperative simulations in plastic and reconstructive surgery. Acta Biomater 2013;9:9036-9048.

Zaborska KE, Wareing M, Austin C. Comparisons between perivascular adipose tissue and the endothelium in their modulation of vascular tone. B J Pharmacol 2017;174:3388-3397.